ELSEVIER

Journal of Non-Crystalline Solids 281 (2001) 139–151

JOURNAL OF NON-CRYSTALLINE SOLIDS

www.elsevier.com/locate/jnoncrysol

Crystallization phenomena in iron-rich glasses

Alexander Karamanov, Mario Pelino *

Department of Chemistry, Chemical Engineering and Materials, University of L'Aquila, 67040 Monteluco di Roio, 67100 L'Aquila, Italy

Received 20 July 2000; received in revised form 24 October 2000

Abstract

In this study, results of the crystallization of iron-rich glasses are summarized. Thermogravimetry (TG)–differential thermal analysis (DTA) were utilized to explain the phase formations and the surface oxidation of FeO to yield Fe_2O_3. The crystal phases fraction was evaluated utilizing X-ray diffraction analysis (XRD). Low angle XRD technique was used to investigate the distribution of the crystal phases on the surface and in the bulk as a function of the heat treatment. Transmission electron microscopy (TEM) was employed to detect the evolution of the crystalline structure and to determine the variation of the residual glass composition. The crystallization kinetics were investigated in isothermal conditions by measuring the variation of the density. The activation energy of crystal growth was calculated using isothermal and non-isothermal methodologies. The values of 377 and 298 kJ/mol were obtained for the temperature ranges 620–660°C and 720–780°C, respectively. Similar values, 368 and 321 kJ/mol, were estimated for the energy of viscous flow in the same temperature ranges. The results indicate that magnetite and pyroxene are the main crystal phases and that the kinetics of pyroxene formation can be explained as growth on a fixed number of magnetite nuclei. In powder samples, heat-treated in air, the crystallization is inhibited by the surface oxidation of Fe^{2+} to yield Fe^{3+} and a layer of haematite is formed on the surface.

1. Introduction

Glass-ceramic materials have a number of outstanding characteristics in comparison with the traditional ceramics and glasses, which determine their application in advanced technology as well as in electronics and medicine [1,2]. However, due to the high cost of some of the raw materials (Li_2O, B_2O_3, etc.), and the high melting temperatures or special melting conditions, glass-ceramics are relatively expensive materials.

It is possible to produce glass-ceramics using cheap raw materials or wastes with low melting temperatures and shorter production cycles, finding wide application in the building industry. Slagsitalls glass-ceramics, produced in the former Soviet Union, were made out of metallurgical slags [3,4] and a number of similar products were developed in other countries [1,4–6].

Products from fused rocks (petrurgy) [7–15] had a wide market and can be considered as predecessors of the glass-ceramic technology. In these materials, an uncontrolled crystallization takes place during cooling and, as a result, a course-grained structure is obtained. Typical of petrurgy are the iron-rich compositions, produced by melting and casting or fibring basalt rocks and containing as much as 10–15 wt% iron oxides [16].

* Corresponding author. Tel.: +39-0862 434 224; fax: +39-0862 434 233.

E-mail address: pelino@ing.univaq.it (M. Pelino).

0022-3093/01/$ - see front matter
PII: S0022-3093(00)00436-1

Iron-rich glasses and glass-ceramics somewhat similar to natural basalt were developed for nuclear waste disposal, because during vitrification the radioactive nuclides are incorporated in the chemically stable glass network [17–22]. More recently, glasses with an iron content of up to 30%, were developed to stabilize some hazardous industrial wastes and recycle the product in the glass or glass-ceramic markets. The wastes subjected to vitrification were jarosite and goethite [23–36], arising from the hydrometallurgy of zinc ores, electric arc furnace dusts collected in the baghouse filter of the electric arc steel production [37–41], as well as some other iron-rich industrial wastes [4,42–44].

Special magnetic glass-ceramics with an extremely high iron content were also developed for electronic applications [45–47].

In the glasses, iron can exist in both ferrous and ferric forms. The Fe^{3+}/Fe^{2+} ratio depends on the chemical compositions and melting conditions being controlled by the melting atmosphere, i.e., by the presence of oxidizing or reducing agents in the batch [8,15,21,35,41]. FeO is a typical modifying oxide while Fe_2O_3 is intermediate, so that the ratio Fe^{3+}/Fe^{2+} influences the viscosity curve and the liquidus temperature. The ferric/ferrous ratio also affects the spinel and pyroxene formation, the rate of crystallization and the final properties of the glass-ceramics.

In the crystallization of iron-rich compositions some typical features are observed. The compositions with high iron content are peculiar since they show a tendency to spontaneous crystallization and in some cases the amorphous structure can be obtained only after quenching in water (glass frit) [28,38,41]. The initial melts are characterized by a high liquid immiscibility [8,12,24,28,33], one of the liquid phases is richer in iron and promotes the formation of the spinels as the initial crystal phase [8,12,20,29,33]. By prolonged thermal treatment the pyroxene solid solution precipitates on the spinel (magnetite, franklinite, chromite) crystals, which act as nuclei for the crystallization.

Another peculiarity of iron-rich glasses is the surface oxidation of Fe^{2+} to yield Fe^{3+} when the samples are heat-treated in air. This phenomenon is a function of the specific surface, decreases the crystallization ability and leads to hematite formation on the surface [27,32,33,46].

The present work is a review of the results of investigations carried out on bulk and surface crystallization in iron-rich glasses made up of zinc hydrometallurgy wastes.

2. Experimental

The glass compositions were prepared by mixing jarosite waste from hydrometallurgy of zinc, granite waste, glass cullet, quartz sand, limestone and Na_2CO_3. The melting was carried out at 1400–1450°C utilizing alumina crucibles. Part of the melts was quenched in water and the frit obtained was broken and sieved. The other part of the melt was poured in a stainless steel mould, annealed and then cut into small specimens for subsequent thermal treatment. The raw material characterizations and the melting conditions were reported elsewhere [26,29,32]. Table 1 reports the chemical compositions, measured by a Spectro-Xepos X-ray fluorescence apparatus, of the jarosite sample, granite-scraps and glass cullet and the corresponding glass compositions used in this work and labeled **G1** and **G2**. The reported associated error is evaluated by the instrument. **G1** was prepared for tile production by casting [26,29] while **G2** for sinter-crystallization of the glass frit [32]. Iron oxides are presented as Fe_2O_3.

Different isothermal and non-isothermal treatments were carried out using powder and bulk glasses. The crystalline phases formed were determined by the X-ray diffraction analysis (XRD) technique (Philips PW1830 apparatus and CuK_α radiation). The crystalline fractions developed during the thermal treatment were evaluated comparing the areas of the amorphous and crystalline phases in the XRD spectra [48]. The ratio between the phases was estimated using the relative intensities of the major peaks [49]. Low angle XRD analysis was employed to highlight the phases on the surface of the glass.

The crystalline fraction was also evaluated by measuring the change of density between the parent glass and the heat-treated sample. For this series of tests, a He displacement Pycnometer

Table 1
Chemical compositions of jarosite waste, granite-scraps, glass cullet and parent **G1** and **G2** glasses in (wt%)

	Jarosite waste	Granite-scraps	Glass cullet	**G1**	**G2**
SiO_2	3.7 ± 0.05	70.2 ± 0.21	72.5 ± 0.23	52.9 ± 0.19	53.8 ± 0.21
Al_2O_3	0.3 ± 0.04	12.1 ± 0.31	0.5 ± 0.04	4.1 ± 0.11	3.7 ± 0.09
Fe_2O_3	49.3 ± 0.04	1.6 ± 0.01	0.1 ± 0.01	24.1 ± 0.03	21.7 ± 0.03
CaO	0.1 ± 0.01	5.2 ± 0.06	8.7 ± 0.11	5.2 ± 0.09	8.7 ± 0.10
MgO	0.2 ± 0.06	0.6 ± 0.10	4.0 ± 0.31	1.8 ± 0.22	0.2 ± 0.05
ZnO	5.6 ± 0.04	–	–	2.7 ± 0.09	2.4 ± 0.08
PbO	3.6 ± 0.02	–	–	1.7 ± 0.01	1.5 ± 0.01
Na_2O	–	2.9 ± 0.27	13.4 ± 0.61	6.4 ± 0.45	6.9 ± 0.43
K_2O	–	3.3 ± 0.07	0.2 ± 0.01	1.1 ± 0.05	1.0 ± 0.05
L.O.I.	37.2 ± 0.43	4.1 ± 0.34	–	–	–

(AccyPyc 1330) was utilized. The experimental associated error to the measurements, employing a 3–4 g glass sample, was evaluated as ± 0.001 g/cm^3.

The oxidation process of Fe^{2+} to yield Fe^{3+} was investigated by thermal gravimetry (Cahn 1000 apparatus). In this series of experiments about 4 g of powder sample were suspended in the microbalance and heated in air atmosphere.

The crystallization kinetics were investigated in non-isothermal conditions by means of differential thermal analysis (DTA) technique. About 100 mg of powder sample (122–212 μm particle size) were used in air and nitrogen atmospheres. The experiments were carried out in 'Netzsch STA 409' apparatus at 5, 10, 15 and 20°C/min heating rates. DTA analyses were also carried on bulk samples in air.

Transmission electron microscopy (TEM) (a Philips CM 200 operating at 200 keV + EDS) was employed to investigate the phase formation. For these studies, the samples were thermally treated at different temperatures and times and then crushed and sieved to obtain a very fine fraction and deposited on a copper–carbon grid. TEM images were used to identify particles with well-defined crystalline structure. The EDS analyses highlighted the variation in the composition of the amorphous and crystalline phases during the thermal treatment.

The viscosity–temperature curve of **G1** glass was estimated by carrying out two series of experiments: the glass transition temperature, T_g, and the dilatometric softening point, T_w, were obtained using a 'Netzsch 402 ED' differential dilatometer at 5°C/min heating rate; the viscosity in the high temperature region, 1200–1320°C, was measured by a rotational viscosimeter.

3. Methodology

3.1. Evaluation of the crystalline fraction by density measurements

Glass-ceramics may be considered as composite materials made up of different crystalline phases and residual glass, so the volume of glass-ceramics is an additive function of the volumes of the vitreous and crystalline phases present.

The crystallization process in the glass-ceramics is connected with volume changes, which are related to the degree of conversion [50,51]. The change of density during crystallization process, related to the volume variation, can be used to estimate the degree of crystallization using the following relation:

$$\frac{100}{\rho_{gc}} = \frac{(100 - x)}{\rho_{g(r)}} + \frac{x}{\rho_{cr}}, \tag{1}$$

where x is the percentage crystal phase, ρ_{gc} is the density of the glass-ceramics, $\rho_{g(r)}$ is the density of the residual glass and ρ_{cr} is the density of the crystal phase formed.

When the parent glass has the same composition as the crystal phase formed, there are no

changes in the residual glass compositions and $\rho_{g(r)}$ is identical to the density of the parent glass ρ_g.

However, during the crystallization of the commercial glasses, the composition of the residual glass, $g(r)$, changes during crystallization, so in order to estimate the percentage of crystal phase formed, some assumptions must be made [30].

Since during crystallization only a portion of the parent glass is transformed in a crystalline phase it can be assumed that the volume of the parent glass (V_g) consists of two parts: $V_{g(c)}$ – with the composition as the crystal phase which is going to be formed and $V_{g(r)}$ – with the composition of the residual glass. So the following relation, similar to Eq. (1), can also be written for the parent glass:

$$\frac{100}{\rho_g} = \frac{(100-x)}{\rho_{g(r)}} + \frac{x}{\rho_{g(cr)}}, \tag{2}$$

where ρ_g is the density of the parent glass and $\rho_{g(cr)}$ is the density of the hypothetical glass with the composition of the crystal glass.

By combining Eqs. (1) and (2), $\rho_{g(r)}$ is eliminated and the percentage crystal phase (x) can be obtained through the relation

$$x = 100\frac{1/\rho_g - 1/\rho_{gc}}{1/\rho_{g(cr)} - 1/\rho_{cr}}. \tag{3}$$

The applicability of this equation depends on the difference between the density of the amorphous phase, $\rho_{g(cr)}$ and the corresponding crystalline phase ρ_{cr} and on the accuracy of the density measurements. For magnetite and pyroxene, the values of $1/\rho_{g(cr)} - 1/\rho_{cr}$ are extremely high and, as a result, the density difference between initial glasses and final glass-ceramics in iron-rich compositions is about 0.15–0.25 g/cm^3. This allows, by using a He displacement Pycnometer, the detection of differences of about 1–2% crystal phase in the crystallized samples.

A detailed description of the methodological approach and application to the crystallization of iron-rich glasses is reported elsewhere [30].

3.2. Crystallization kinetics by DTA measurements

The crystallization kinetics in glasses are usually investigated by the Kolmogorov, Johnson, Mehl, Avrami (KJMA) equation in the form [1,51]

$$\alpha(\tau) = 1 - \exp(-\text{const.}\, I_0 U^{n-1}\tau^n), \tag{4}$$

where $\alpha(\tau)$ is the degree of transformation at time τ, I_0 is the rate of steady-state nucleation, U is the rate of crystal growth and n is the Avrami parameter, an integer number which depends on the growth direction number and the mechanisms of nucleation and crystal growth.

DTA is widely used for the kinetics investigation in glasses, for evaluation of the crystallization activation energy as well as for the estimation of the reaction order, i.e., the Avrami parameter, n, in Eq. (4) [52]. In the case when there is no nucleation during DTA run, the activation energy of crystal growth, E_c, can be estimated carrying out DTA experiments at different heating rates, by using the Kissinger equation [53]

$$\ln(\phi/T_p^2) = -E_c/RT + \text{const.}, \tag{5}$$

where T_p is the crystallization peak temperature of the DTA trace, ϕ is the heating rate and R is the gas constant. A plot of $\ln(\phi/T_p^2)$ vs. $1/T_p$ is a line, whose slope corresponds to E_c.

The Avrami parameter, n, can be determined by Ozawa's method using the following equation [54]:

$$\left.\frac{d[\ln(-\ln(1-\alpha))]}{d(\ln\phi)}\right|_T = -n, \tag{6}$$

where α is estimated by evaluating the partial area of the crystallization peak from exotherms, obtained at different heating rates and at a fixed temperature, T.

The value of n can also be estimated by the Augis and Bennett [55] equation

$$n = (2.5/\Delta w)(RT_p^2/E_c), \tag{7}$$

where Δw is the width of the crystallization peak at half height. In this case the Avrami parameter can be evaluated by a single DTA experiment if the activation energy has been previously obtained by other methods.

4. Results and discussion

4.1. Bulk crystallization

With the aim of obtaining information on the crystallization ability of the parent glass and temperature interval of transformation, DTA were carried out in the 20–1200°C temperature range. In Fig. 1 the corresponding DTA plots of the **G1** and **G2** bulk samples obtained at 10°C/min heating rate are reported.

The T_g of the **G1** and **G2** glasses occurs at 560°C and 570°C, respectively, temperatures which are typical for iron-rich glass composition [7,12,17,28]. The formation of crystalline phases is represented by the occurrence of a single exothermal peak, having its maximum at 780°C for **G1** and 805°C for **G2**, respectively. The melting endo-peaks, however, highlight that two phases melt at different temperatures in both samples. For **G1** composition the temperatures of the endo-peaks are at 1080°C and 1120°C while for **G2** they are lower – at 1025°C and 1070°C, respectively. It was previously demonstrated [32] that for **G2** composition, the first peak corresponds to the melting of pyroxene, which represents the major crystalline phase and the second one to the melting of magnetite.

In isothermal conditions the crystallization behavior was investigated by measuring the density change as a function of different heat treatments. Fig. 2 shows the density variation and the corresponding percentage of crystal phase evaluated according to Eq. (3) of **G1** samples, heat-treated for 1 and 10 h holding time at different temperatures. For 1 h heat treatment the density variation, i.e., the crystallization of the glass, starts at 620°C and reaches its maximum at 700°C. For 10 h heat treatment the beginning of the crystallization occurs at 600°C, the degree of transformation is higher and its maximum is obtained at 660°C.

By treating the glass at temperatures higher then 680–700°C the density, i.e., the degree of transformation, decreases. The densities, measured after 1 and 10 h, are similar so that the percentages of crystallization shown in the figure can be considered as the maximum obtainable at these temperatures. Similar behavior was reported for other iron-rich compositions [11,31,46].

Fig. 3 shows the variation of the crystal phase percentage as a function of time at different constant temperatures (620°C, 640°C and 660°C) [29]. The maximum density was obtained after heat treatment up to 20 h at 660°C and resulted in being 3.04 g/cm^3, corresponding to about 55% crystal phase. Assuming that this value corresponds to the maximum degree of transformation $\alpha = 1$ in Eq. (4), the Avrami parameter, n, was obtained from the slope of the linear regression by plotting the

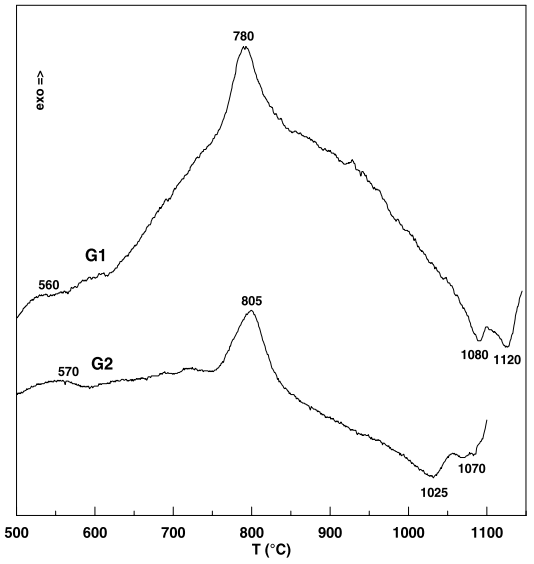

Fig. 1. DTA traces of **G1** and **G2** bulk samples.

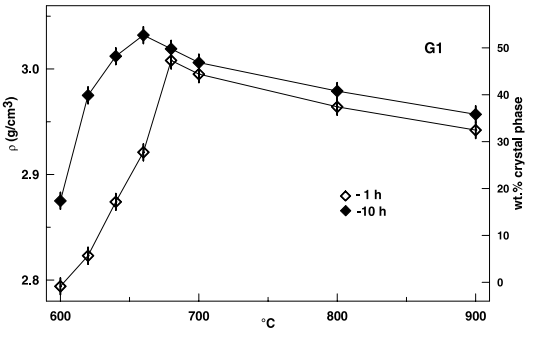

Fig. 2. Variation of the density after 1 and 10 h heat treatment at different temperatures.

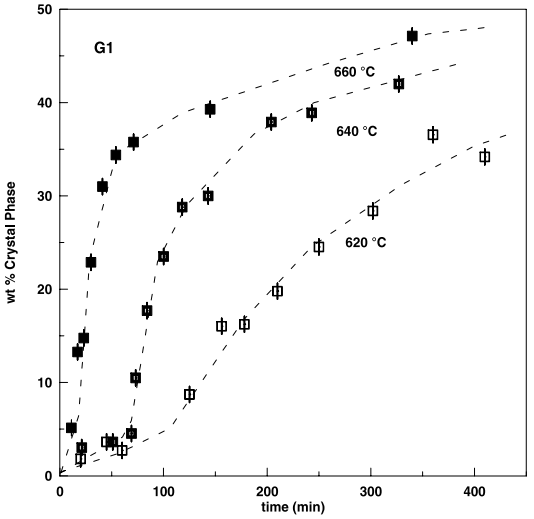

Fig. 3. Percentage of crystal phase formed as a function of the time in **G1** composition at 620°C, 640°C and 660°C.

value of $\ln\ln[1/(1-\alpha)]$ as a function of $\ln\tau$. The obtained n values for 620°C, 640°C and 60°C are 1.53, 1.52, and 1.44, respectively.

Kinetics results were also obtained for the crystallization of **G2** composition [32]. Fig. 4 reports the kinetics curve, obtained by density measurements after heat treatments at 680°C. In this case an n value of 1.36 was obtained.

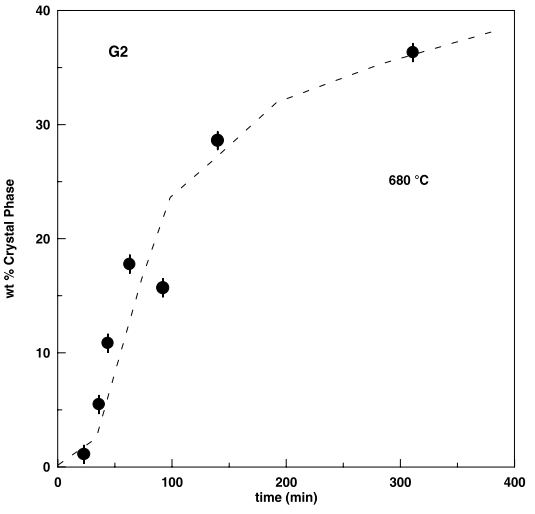

Fig. 4. Percentage of crystal phase formed as a function of the time in **G2** composition at 680°C.

All the obtained values for the Avrami parameter, n, are near 1.5 which can be related to the diffusion-controlled three-dimensional growth taking place on a fixed number of nuclei or, eventually, to simultaneous nucleation process and one-directional crystal growth.

In order to assess the eventual presence of a nucleation process, two different series of experiments were carried out using **G1** samples [29]. In the first series, the densities were measured after 1 h heat treatment in the T_g–$(T_g + 60°C)$ temperature range (560–620°C). Then the 'nucleated' sample was heat-treated for 30 min at 680°C to allow crystallization and the density was measured again. The parent glass sample was directly treated at 680°C for 30 min. No sensible variation of density was induced by the nucleation heat treatments compared to the direct crystallization of the parent glass, so it was concluded that, in the investigated temperature range, no nucleation takes place.

In the second series of experiments, bulk samples were placed in the DTA and treated for 1 h at 600°C, 620°C and 640°C and then the temperature was raised by 15°C/min heating rate. In the three investigated samples, the position of the crystallization peak resulted in being the same as the non-nucleated sample, treated with the same heating rate. These results support the hypothesis that the nucleation process is negligible and that the reaction order, n, for the 620–660°C temperature range can be explained as three-dimensional diffusion-controlled growth on a fixed number of nuclei.

The three-dimensional magnetite and pyroxene structure was also confirmed by TEM observation for different goethite and jarosite glass-ceramics [23,28,29,33]. Fig. 5 shows the dendritic pyroxene structure, precipitated in **G1** composition heat-treated for 3 h at 660°C. Similar results showing a typical dendrite pyroxene crystal were also reported for other iron-rich compositions [8,11,12,18,19].

TEM of the parent glass was employed to investigate the variation of compositions among the residual glass and crystal phases during the crystallization process. By observing particles of the parent glass and collecting the fluorescence emission of the main elements, i.e., Si, Fe, Zn, Ca, Na,

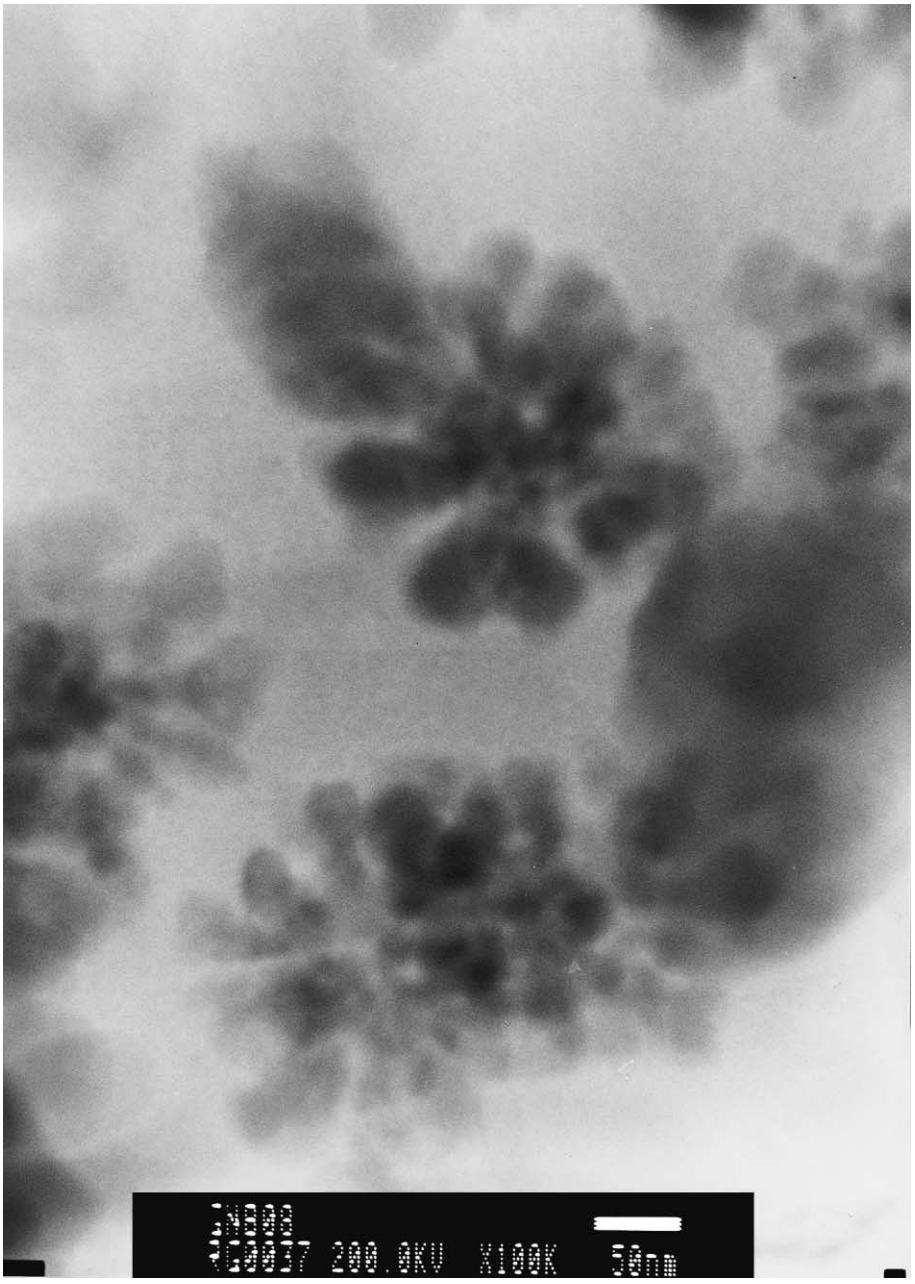

Fig. 5. TEM picture of **G1** composition after 3 h heat treatment at 660°C.

Pb, a map of the distribution in the glass grain has been obtained [24,36]. The glass showed that Fe and Zn are concentrated in specific areas while the other elements are uniformly distributed in the matrix, suggesting that liquid–liquid separation may occur during the cooling of the melt. These areas become, during the thermal treatment, sites for the precipitation of magnetite (Fe_3O_4) and franklinite ($ZnFe_2O_4$). In the surrounding zones, where the Si concentration is higher the formation

of the pyroxene is favored after spinel precipitation. After the crystallization is completed Pb and Na are concentrated in the residual glassy phase, thus affecting the leaching properties of the glass-ceramics.

The formation of the crystal phases in **G1** composition was also investigated by XRD analysis. Fig. 6 shows the spectra of the parent glass before and after thermal treatments at 660°C for different times.

The parent glass shows an amorphous spectrum with some traces of magnetite formation. However, the peaks are not sharp and the 'path' is very wide so that they could be related to a liquid–liquid separation with the presence of an iron-rich phase, i.e., not yet well-arranged magnetite structure. After 20 min heat treatment at 660°C the magnetite peaks become sharper and the amount of crystalline phase formed in the sample can be evaluated as about 7–9 wt%. After 40 min of heat treatment the beginning of the pyroxene phase formation is well evident. After 3 h thermal treatment, the crystallization is completed and pyroxene represents the major crystal phase in the glass-ceramic.

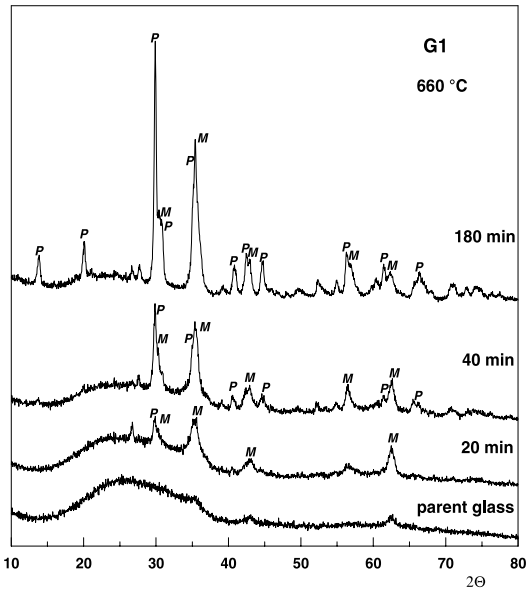

Fig. 6. XRD spectra of **G1** bulk samples heat-treated at 660°C for different times.

These results confirm that the phase transformation starts with magnetite formation and that the pyroxene crystallization is influenced by the magnetite phase, i.e., the magnetite crystals act as nuclei for the pyroxene crystal phase precipitation. The spectra highlighted that the magnetite peak intensity does not sensibly increase with a prolonged thermal treatment (more than 20 min) while pyroxene formation occurs after magnetite precipitation and increases with time up to 180 min.

XRD analysis of **G1** bulk glass was also made after heat treatment at 740°C [34]. The result confirmed that the total amount of crystal phase decreases with the increasing of the temperature. The maximum amount of crystal phases for this temperature corresponds to about 9–11% magnetite and about 34–36% pyroxene. The analysis of the spectrum after 3 h at 660°C gives about 8–10% magnetite and 43–45% pyroxene. It can be concluded that the increasing of the heat treatment temperature leads to the decreasing of the amount of pyroxene phase while the amount of magnetite phase does not changes. Similar results have been reported for some basalt compositions [11].

It might be assumed that, for similar compositions, the crystallization thermal cycle can be carried out by a single isothermal step being the optimum heat treatment 60–90 min at 680–720°C yielding a 50–60 wt% crystal phase.

4.2. Surface crystallization in powder and bulk samples

In general, the mechanisms of crystal growth are similar for surface and bulk [56,57], so the differences in the crystallization depend on the number of nuclei formed and their distribution [58]. However, the furnace atmosphere might play an important role in the surface crystallization by modifying the composition of the surface [56,57].

In iron-rich glasses, the initial Fe^{3+}/Fe^{2+} ratio generally depends on the chemical compositions and melting conditions [8,35,44], but due to the surface oxidation process ($Fe^{2+} \Rightarrow Fe^{3+}$) the ratio on the surface might be consistently different than in the bulk thus influencing the phase transformation.

In previously investigated iron-rich goethite and jarosite glasses melted in electric or gas furnaces, the Fe^{3+}/Fe^{2+} ratio was estimated between 7 and 10 [25,29,35]. Similar values were reported for different basalt [8] and magnetic glass-ceramics [45], melted at 1400–1450°C in air for times up to 10–15 h.

In Figs. 7(a) and (b) the XRD spectra of a bulk (**B**) sample, heat-treated with 5°C/min heating rate up to 950°C and held at 950°C for 24 h are shown, respectively. The first spectrum yielded about 43–45 pyroxene and 3–5 magnetite while the second about 35–37 pyroxene and 8–10 magnetite crystal phases, respectively. Considering similar results reported in the literature [11] it was concluded that at high temperatures (900–1000°C) re-crystallization of pyroxene yielding magnetite takes place.

Figs. 7(c) and (d) show the XRD spectra of powder, **P**, samples, heat-treated with 5°C/min heating rate up to 950°C and held at 950°C for 24 h, respectively. The first spectrum yielded about 31% crystal phase, only pyroxene; the second spectrum yielded 38% crystal phase and the formation of hematite due to the oxidation of Fe^{2+} is evident. The intensities of the pyroxene peaks in both **P** samples are similar.

TG–DTA analysis confirmed the different crystallization behaviors of bulk and powder **G2** samples. The TG–DTA were carried out with 10°C/min heating rate using powder samples heat-treated in air and nitrogen atmospheres and bulk sample heat-treated in air [32]. The results for powder sample **(P)** are reported in Fig. 8. The TG trace of the **P** sample in air shows a detectable increase of weight, about 0.5%, taking place after 620°C. This weight change is connected with an exothermal effect having its maximum at 720°C. The crystallization peak occurs, in the same graph, at 875°C, while two melting points are noticeable at 1080°C and 1180°C, respectively. When the **P** sample is heat-treated in N_2 atmosphere no TG variation is detected and the only exothermal peak is the one relative to the crystallization. The melting pyroxene point in this case occurs at a lower temperature (1025°C). Finally, when a bulk sample was heat-treated in air no TG variation

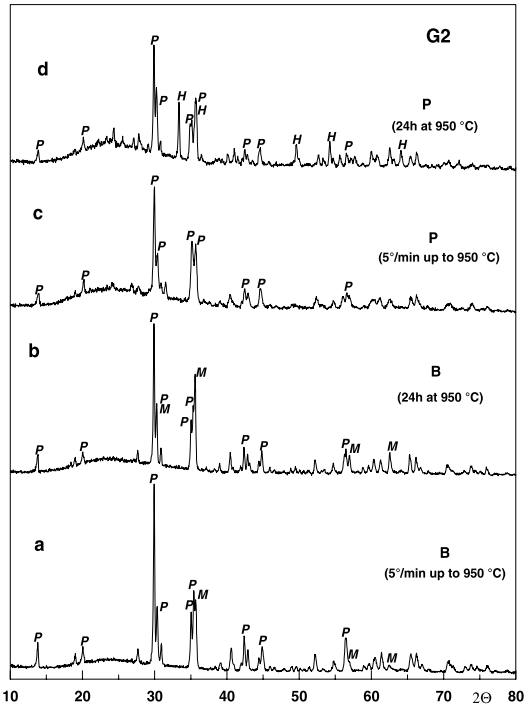

Fig. 7. XRD spectra of bulk, **B**, and powder, **P**, **G2** samples heat-treated at 950°C.

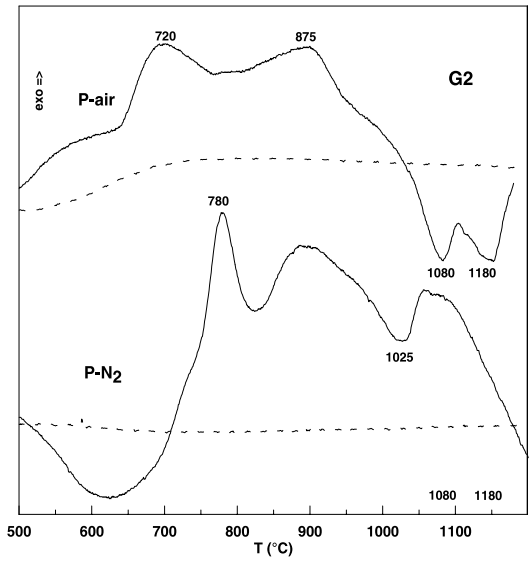

Fig. 8. DTA (solid line) and TG (dashed line) of **G2** powder samples, heat-treated in air (**P**–air) and nitrogen (**P**–N_2) atmospheres.

appeared in the trace; the crystallization exo-peak occurs at 805°C and the melting pyroxene endo-peak at 1025°C, i.e., the same temperature as in the powder sample heat-treated in N_2. DTA traces are reported in Fig. 1.

In order to highlight the oxidation kinetics, isothermal treatments were carried out at 630°C and 680°C with 0.3–0.5 mm **G2** glass powder fraction and the differential weight gain was recorded as a function of the time [35]. The results are plotted in Fig. 9 which shows that by increasing the temperature, the weight gain increases rapidly in the first 60 min and then assumes an asymptotic behavior. No appreciable weight gain was detected by heat treatments below T_g (24 h at 540°C), temperatures at which the diffusion process and structural changes are practically inhibited. By plotting the weight gain as a function of the square root of time, straight lines were obtained [32], which can be related to the diffusion of Fe^{2+} from the bulk to the surface of the glass.

The degrees of crystallization for **G2** glass were investigated by measuring the variation of density and by XRD analysis for **P** and **B** samples heat-treated at 680°C. The change of density is negligible for **P** even after up to 500 min heat treatments and the XRD analysis highlighted an amorphous spectrum with some low intensity peaks of magnetite. At the same time, as it is highlighted in Fig. 4 after 400 min heat treatment at 680°C, the crystallization process in **B** sample is complete with a value of about 45% crystal phase.

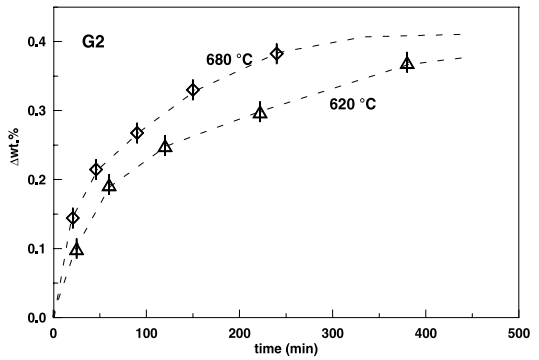

Fig. 9. Differential weight gain as a function of the time of **G2** glass powder.

Low angle XRD method was used to investigate the distribution of the phases formed on the surface (**S**) and on the bulk (**B**) during heating. Fig. 10 shows the spectrum of the surface of a **G2** bulk sample, heat-treated for 2 h at 680°C and 950°C, and the corresponding spectrum after polishing the surface for about a millimeter. After heat treatment at 680°C the surface layer is still amorphous, while pyroxene formation occurred in the bulk. The comparison of the spectrum after heat treatment at 950°C highlights that hematite is prevalent on the surface of the glass while pyroxene is the main crystal phase in the bulk. Optical

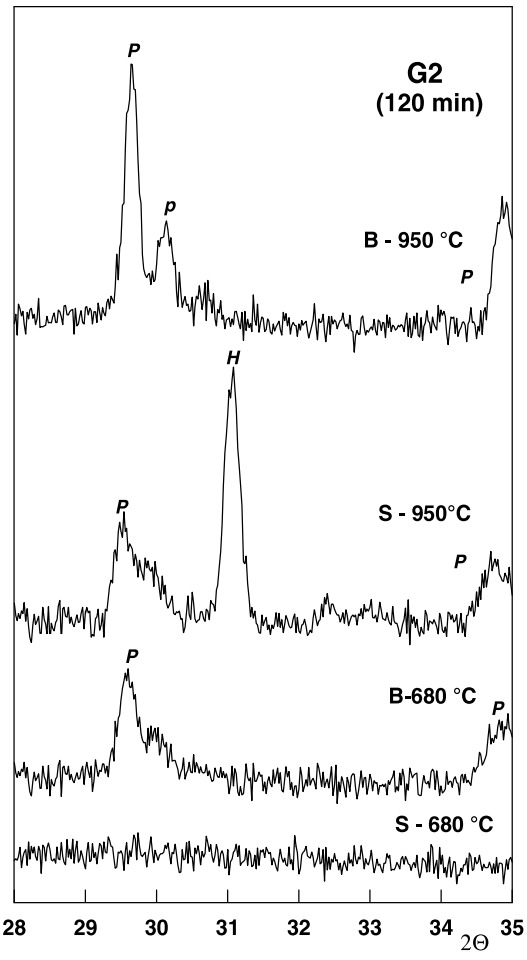

Fig. 10. Low angle XRD of the surface, before (**S**) and after polishing (**B**), of **G2** samples heat-treated at 680°C and 950°C.

[32] and scanning electron [27,33] microscopes confirmed the presence of about 0.1 mm thick hematite phase on the surface of the glasses.

4.3. The activation energy of crystallization

The activation energy of crystal growth on a fixed number of nuclei, E_c, can be evaluated using isothermal kinetics results obtained at different temperatures. In this case, assuming an Arrhenius temperature dependence for the crystal growth rate, i.e., $U = U_0 \exp[-E_c/(RT)]$, Eq. (4) can be written in the form

$$\ln \tau_\alpha = E_c/(RT) + \text{const.}, \tag{8}$$

where τ_α is the time, corresponding to a certain value of α. If the logarithm of τ_α is plotted against $1/T$, the slope yields the E_c/R value. By this method, the E_c value for **G1** composition in the 620–660°C temperature range resulted in being 377 kJ/mol [29].

For the **G1** composition, the activation energy was also evaluated by the Kissinger equations using DTA experiments with little bulk samples carried out at different heating rates. The value obtained by this methodological approach, using Eq. (5) resulted in being 298 kJ/mol [29].

The differences in the E_c values can be explained by considering that the DTA crystallization peaks were observed in the temperature interval 720–780°C, i.e., in a temperature range of about 100°C higher than the one for the isothermal investigations.

The variation of E_c with the increasing of temperature can be related to the temperature dependence of the activation energy of the viscous flow, E_η. E_η was evaluated by viscosity measurements in the low temperature range where no crystallization occurred, i.e., 560–620°C and at temperatures higher than the liquidus. $T_g(\eta(\text{dPa s}) = 10^{13.3})$ [59] and T_w – dilatometric softening point ($\log \eta = 11.3$) [60] were evaluated by dilatometric experiment while in the high temperature region (1200–1320°C) the viscosity was measured by means of a rotational viscometer. The associated error to the dilatometric measurements was evaluated as ±2°C, while for the rotational viscometer measurements of ±4°C. The viscosity–temperature curve was evaluated through Vogel–Fulcher–Tammann (VFT) equation [59,60] using the experimental points. Fig. 11 reports the obtained experimental points and the calculated VFT viscosity curve as function of temperature. Then the activation energy of viscous flow, for different temperature intervals, was calculated using an Arrhenious dependence for E_η [6,60]. The values of 368 and 321 kJ/mol were obtained for the 620–660°C and 720–780°C temperature ranges, respectively, i.e., values in good agreement with the corresponding values of E_c.

The DTA experiments were also employed to estimate the Avrami parameter value [34]. The n value, obtained by the Ozawa method at 750°C was 2.9. Similar n values (between 2.8 and 3.1) were obtained by the Augis and Bennett method for each of the experimental exotherms. All obtained values are near 3, which can be related to a three-dimensional time-independent growth on a fixed number of nuclei. This value is different by n value of 1.5, obtained in the low temperature range (620–660°C).

The difference in the Avrami parameter with the temperature may be related to a change in the diffusion process. It is known that, when the scale of the diffusion field becomes constant, the

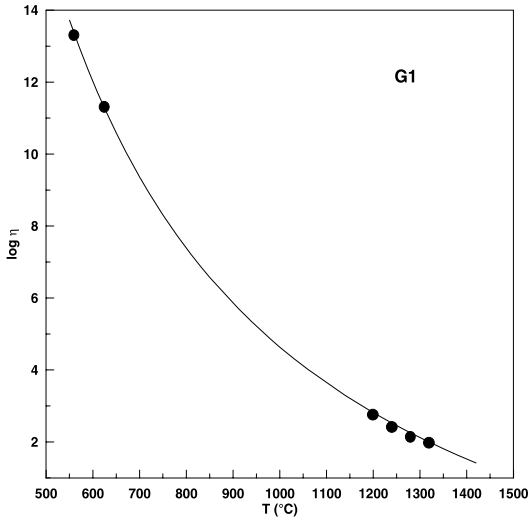

Fig. 11. Viscosity vs. temperature curve for **G1** composition.

diffusion-controlled crystal growth becomes time independent [61]. This is typical of dendritic formation or of fiber-like surface crystallization [62], when the growth is carried out at higher temperatures.

The activation energy of crystal growth, E_c and the reaction order, n were also estimated on powder **G1** glass, carrying out DTA experiments in air, **P**–air, and nitrogen atmospheres,**P**–N_2 [34]. The E_c values of 321 and 319 kJ/mol were obtained for **P**–air and for **P**–N_2, respectively, by using the Kissinger equation (Eq. (4)). It was concluded that the diffusion process connected with the crystal growth is similar when bulk or powder glasses are heat-treated in an air or nitrogen atmosphere.

The Avrami parameter, n, was evaluated by the Ozawa method (Eq. (4)) at 825°C for **P**–air and at 740°C for **P**–N_2, as well as by the Augis and Bennett method (Eq. (4)) for each of the experimental exotherms [34]. The results of both the methods were about 3 for **P**–N_2 sample, which can be related to a three-dimensional time-independent growth on a fixed number of nuclei, i.e., the same result as the value, obtained for **B**–air sample. For **P**–air sample, a n value of about 1.2 was obtained by both methods which correspond to two-dimensional parabolic growth or, alternatively, to one direction time-independent growth.

5. Conclusions

The results of this work throw some light on characteristic crystallization phenomena in iron-rich glasses.

For the investigated compositions the crystallization begins with spontaneous magnetite formation which is favored by the initial liquid–liquid separation; the magnetite crystals become nuclei for the precipitation of major pyroxene phase.

The crystallization kinetics in bulk glasses have been interpreted as a three-dimensional diffusion-controlled pyroxene formation on a fixed number of nuclei. The activation energy of crystal growth on surface and bulk are similar in air and nitrogen atmospheres which indicate similar diffusion processes associated with pyroxene formation.

The surface oxidation of Fe^{2+} to yield Fe^{3+} is connected with diffusion of the iron from the bulk to the surface and leads to a change of the chemical composition. As a result, the crystallization of powder glass in air is inhibited and hematite is formed on the surface samples at high temperatures.

Acknowledgements

The authors are grateful to all the partners of the Brite-Euram-CT94-1018 project; to Dr G. Taglieri, Eng. P. Pisciella and Mrs F. Ferrante for carrying out part of the experimental work.

References

[1] Z. Strnad, Glass-Ceramic Materials, Elsevier, Amsterdam, 1986.
[2] G.H. Beall, in: Reviews of Solid State Science, vol. 3, World Scientific, Singapore, 1989, p. 333.
[3] N. Pavlushkin, P. Sarkusov, L. Orlova, Slagsitalls, Strojiisdat, Moskow, 1977 (in Russian).
[4] M.A. Besborodov, Glass-Ceramic Materials, Nauka i Technika, Minsk, 1982 (in Russian).
[5] R.D. Rawlings, in: Glass-Ceramic Materials-Fundamentals and Applications, Series of Monographs on Material Science, Engineering and Technology, Mucchi Editore, 1997, p. 115.
[6] J. Hlavac, The Technology of Glass and Ceramics: An Introduction, Elsevier, Amsterdam, 1983.
[7] B. Locsei, Molten Silicates and their Properties, Akademiai Kiado, Budapest, 1970.
[8] G.H. Beall, H.L. Rittler, Ceram. Bull. 55 (6) (1976) 579.
[9] A.K. Bandyopadhyay, P. Labarbe, J. Zarzycki, A.F. Wright, J. Mater. Sci. 18 (1983) 709.
[10] C.G. Rouse, S.M. Toffoli, Ceramica 31 (185) (1985) 105.
[11] M. Hidalgo Callejas, J.Ma. Rincon, in: Pask, Eveans (Eds.), Ceramic Microstructures 86, Plenium, New York, p. 117.
[12] V. Znidarsic-Pongarac, D. Kolar, J. Mater. Sci. 26 (1991) 2490.
[13] I. Vicente-Mingarro, J.Ma. Rincon, P. Bowles, R.D. Rawlings, P.S. Rogers, Glass Technol. 33 (2) (1992) 49.
[14] I. Vicente-Mingarro, P. Callejas, J.Ma. Rincon, in: Proceedings of the First European Ceramics Congress, Maastricht, Netherlands, Elsevier, Amsterdam, 1993, p. 2527.
[15] A. Ozturk, in: Proceedings of the 18th International Congress on Glass, American Ceramic Society, San Francisco, California, USA, 1998.
[16] S.A. Morse, Basalts Phase Diagrams, Springler, New York, 1982.

[17] L.A. Chick, R.O. Lokken, L.E. Thomas, Ceram. Bull. 62 (1983) 505.
[18] A. Stalios, R. Batist, in: Proceedings of the Materials Research Society, vol. 50, Elsevier, Amsterdam, 1985, p. 255.
[19] E. Grave, A. Stalious, A. Alboom, J. Nucl. Mater. 171 (1990) 189.
[20] D. Kim, P. Hrma, D. Smith, M. Schweiger, in: G.B. Mellinger (Ed.), Ceramic Transactions, Environmental and Waste Management Issues in the Ceramic Industry, American Ceramic Society, 1994, p. 179.
[21] D. Schreiber, B.K. Kochanowski, C.W. Shreberg, in: G.B. Mellinger (Ed.), Ceramic Transactions, Environmental and Waste Management Issues in the Ceramic Industry, vol. 39, American Ceramic Society, 1994, p. 141.
[22] I.W. Donald, B.L. Metcalfe, R.N. Taylor, J. Mater. Sci. 32 (1997) 5851.
[23] M. Pelino, C. Cantalini, F. Vegliò, P. Plescia, J. Mater. Sci. 28 (1993) 2087.
[24] M. Pelino, C. Cantalini, M. Tazzi, F. Ullu, in: Proceedings of the XX International Mineral Processing Congress, Aachen, Germany, 21–26 September 1997, p. 597.
[25] M. Pelino, C. Cantalini, J.Ma. Rincon, J. Mater. Sci. 32 (1997) 4655.
[26] M. Pelino, Interceram 47 (1) (1998) 22.
[27] J.Ma. Rincon, M. Pelino, M. Romero, in: Proceedings of the First National Congress Valorization and Recycling of Industrial Wastes, L'Aquila, Italy, 7–10 July 1997, p. 169.
[28] M. Romero, M. Rincon, J. Euro. Ceram. Soc. 18 (1998) 153.
[29] A. Karamanov, C. Cantalini, M. Pelino, A. Hreglich, J. Euro. Ceram. Soc. 19 (1999) 527.
[30] A. Karamanov, M. Pelino, J. Euro. Ceram. Soc. 19 (1999) 649.
[31] A. Karamanov, P. Pisciella, M. Pelino, J. Euro. Ceram. Soc. 19 (1999) 2641.
[32] A. Karamanov, G. Taglieri, M. Pelino, J. Am. Ceram. Soc. 82 (1999) 3012.
[33] M. Romero, J.Ma Rincon, J. Am. Ceram. Soc. 82 (1999) 1313.
[34] A. Karamanov, P. Pisciella, M. Pelino, J. Euro. Ceram. Soc. 20 (2000) 2233.
[35] A. Karamanov, P. Pisciella, C. Cantalini, M. Pelino, J. Am. Ceram. Soc. 81 (2000) 3153.
[36] P. Pisciella, S. Crisucci, A. Karamanov, M. Pelino, Waste Manage. 21 (2001) 1.
[37] L. Gress, A. Sarko, Iron Steel Eng. 8 (1993) 38.
[38] B.E. Roger, J.E. Schlobohm, Iron Steel Eng. 4 (1993) 23.
[39] J. Aota, L. Morin, S.A. Mikhail, T.T. Chen, D.T., Waste Process. Recyc. 9 (1995) 335.
[40] D. Ionescu, T.R. Meadowcrof, P.V. Bar, Waste Process. Recyc. 9 (1995) 351.
[41] S. Crisucci, A. Karamanov, P. Pisciella, M. Pelino, in: Proceedings of the IIth National Congress on Valorization and Recycling of Industrial Wastes, L'Aquila, Italy, 5–8 July 1999, p. 107.
[42] E.J. DeGuire, S.H. Risbud, J. Mater. Sci. 19 (1984) 1760.
[43] N.I. Minco, N.F. Jernovaja, Phys. Chem. Glasses 17 (1991) 286 in Russian.
[44] E. Kuleva, L.A. Orlova, O.N. Borisov, M. Gulikin, in: Proceedings of the XVIIIth ICG, Am. Ceram. Soc., 5–8 July 1998, San Francisco, USA.
[45] C.G. Rouse, J. Williams, in: Special Ceramics 6, vol. 6, British Ceramic Research Association, 1975, p. 91.
[46] S. Lee, Y. Choi, J. Mater. Sci. 32 (1997) 431.
[47] U. Lembke, A. Hoell, R. Kranold, R. Muller, W. Schuppel, A. Wiedenmann, in: Proceedings of the XVIIIth ICG, Am. Ceram. Soc., 5–8 July 1998, San Francisco, USA.
[48] H. Kim, R. Rawligs, P. Rogers, Br. Ceram. Trans. J. 88 (1989) 21.
[49] H.P. Klug, L.E. Alexander, X-ray Diffraction Procedures for Polycrystaline and Amorphous Material, Wiley, New York, 1974.
[50] I. Gutzow, J. Crystal Growth 48 (1979) 589.
[51] I. Gutzow, J. Shmelzer, The Vitreous State – Structure, Thermodynamics, Rheology and Crystallisation, Springer, Berlin, New York, 1995.
[52] C.S. Ray, D.E. Day, Ceramic Transactions, in: Nucleation and Crystallization in Liquids and Glasses, Am. Ceram. Soc. 30 (1992) 207.
[53] H.E. Kissinger, Anal. Chem. 29 (1957) 1702.
[54] T. Ozawa, Polymer 12 (1971) 150.
[55] J.A. Augis, J.E. Bennett, J. Therm. Anal. 13 (1978) 283.
[56] E.D. Zanotto, Ceramic Transactions, in: Nucleation and Crystallization in Liquids and Glasses, Am. Ceram. Soc. 30 (1992) 65.
[57] G. Partrige, Glass Technol. 28 (1987) 9.
[58] I. Gutzow, R. Paskova, A. Karamanov, J. Schmelzer, J. Mater. Sci. 33 (1998) 5265.
[59] H. Sholze, Glass, Nature Structure and Properties, Springer, Berlin, 1995.
[60] A. Feltz, Amorphe und Glasartige Anorganische Festkorpen, Academie-Verlag, Berlin, 1983.
[61] N.H. Christensen, A.R. Cooper, B.S. Rawal, J. Am. Ceram. Soc. 56 (1973) 557.
[62] D.R. Uhlmann, E.V. Uhlmann, Ceramic Transactions, in: Nucleation and Crystallization in Liquids and Glasses, Am. Ceram. Soc. 30 (1992) 109.